Extended data Fig 1: HHV-6A reactivation induce mitochondrial fission via the p53/Drp1 axis.

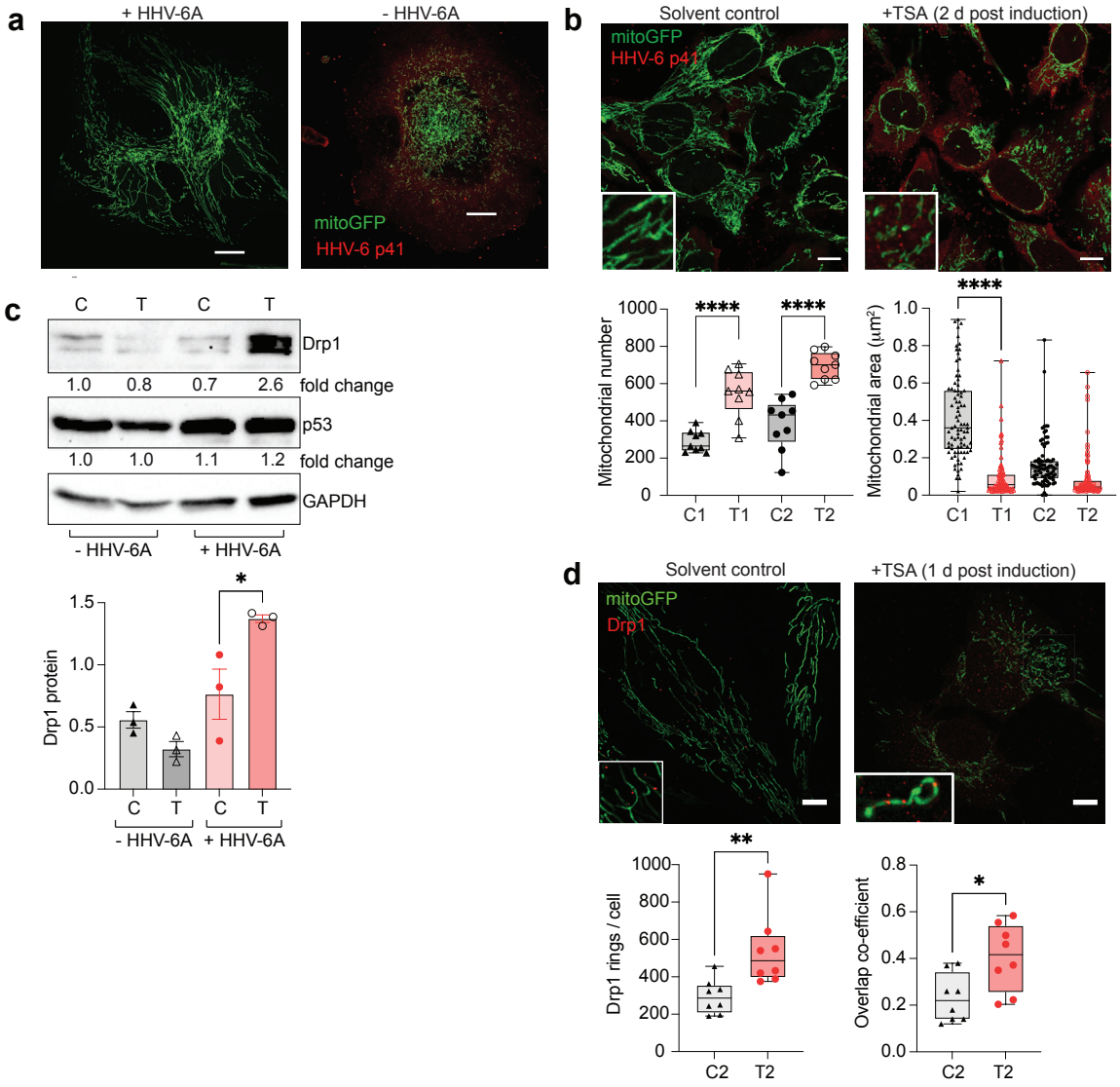

a. Mitochondria in lytic HHV-6A infected primary HUVEC cells expressing soluble GFP within mitochondrial lumen (mitoGFP). HHV-6 p41 protein was tested for virus infection. Representative images from 3 independent experiment. n=3. **b.** HHV-6A reactivation in U2-OS cells expressing mitoGFP and carrying latent HHV-6A genome was stimulated for 24 or 48 h using TSA (T) or DMSO as solvent control (C). Cells were either fixed after one (C1 or T1) or two (C2 or T2) days of treatment and studied using confocal microscopy. Representative confocal images of cells two days post treatment are shown. Mitochondria in confocal images are presented as box and whiskers plot. Immunostaining against HHV-6 p41 protein was carried out to identify virus reactivation. n= 9 cells per conditions. **c.** Virus reactivation in U2-OS cells with or without latent HHV-6A was induced for 48 h using TSA (T) or solvent control (C). Changes in Drp1 and p53 protein expression were quantified using densitometric analysis of immunoblots. GAPDH normalized Drp1 protein levels are presented as a bar diagram. n=3 per condition. **d.** Structured illumination microscopy (SIM) was used to quantify Drp1 rings around mitochondria. Cells from the above experiment were processed for SIM after Drp1 immunostaining. Enlarged Drp1 rings are shown within white boxes. Drp1 rings per cell together with Pearson's overlap coefficient were quantified from the obtained images. Scale bars represent 10 µm. Data are mean ± s.e.m. *P ≤ 0.05, **P ≤ 0.005, ****P ≤ 0.0001, two-way ANOVA with Tukey's multiple comparisons test, two-tailed Mann–Whitney U-test (b-d).

Extended data Fig 2: HHV-6A lytic infection and reactivation impairs miR-30 processing.

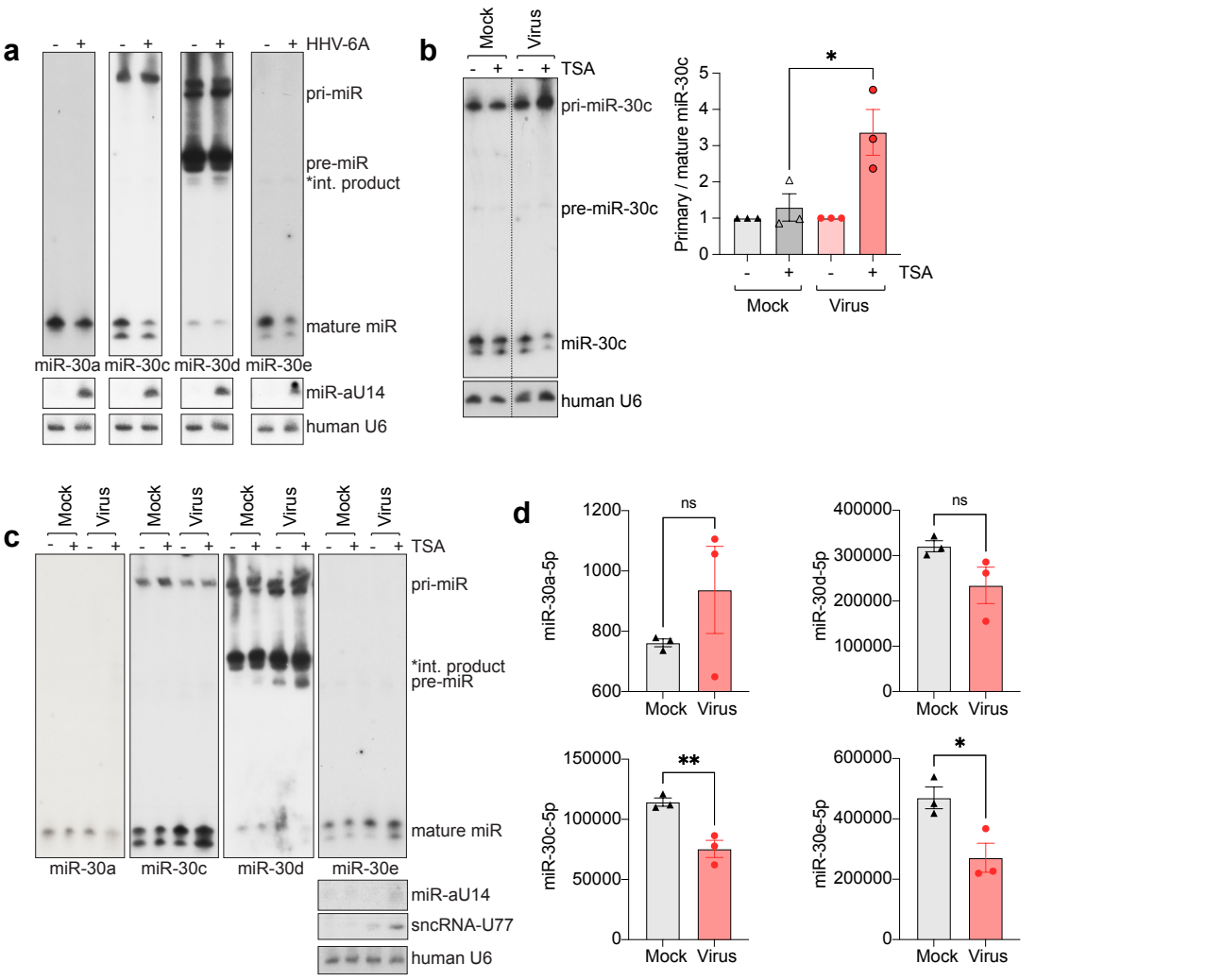

a. HSB-2 cells were infected for 48 h with HHV-6A for lytic virus infection. Total RNA from mock- and HHV-6A-infected cells was analyzed by Northern blotting. **b.** HHV-6A reactivation in U2-OS cells carrying latent HHV-6A was induced for 48 h using TSA. Cells without HHV-6A served as mock. miR-30c levels were studied by Northern blotting. A probe against human U6 was used as loading control. The pri-miR-30c to mature miR-30c ratios, as determined by densitometric analysis, are shown as bar diagrams. n=3. **c.** Virus reactivation of U2-OS cells carrying latent HHV-6A was induced for 48 h using TSA. miRNA expression was analyzed by Northern blotting. Blots for human U6, miR-aU14 and sncRNA-U77 are shown only once as the same blot was stripped and used for reprobing against multiple miR-30 family members. All the images shown are from a single gel. HHV-6 miR-aU14 and sncRNA-U77 was probed to confirm virus reactivation. **d.** Normalized read counts of miR-30 family members from HSB-2 cells either mock infected (-) or infected with HHV-6A (+). n=3. Data are mean ± s.e.m. ns, $P > 0.05$, $*P \leq 0.05$, $**P \leq 0.005$, two-way ANOVA with Tukey's multiple comparisons test (b), two-tailed Mann–Whitney U-test (d).

Extended data Fig 3: HHV-6A miR-aU14 shows sequence complementarity to hairpin loop of miR-30 family members.

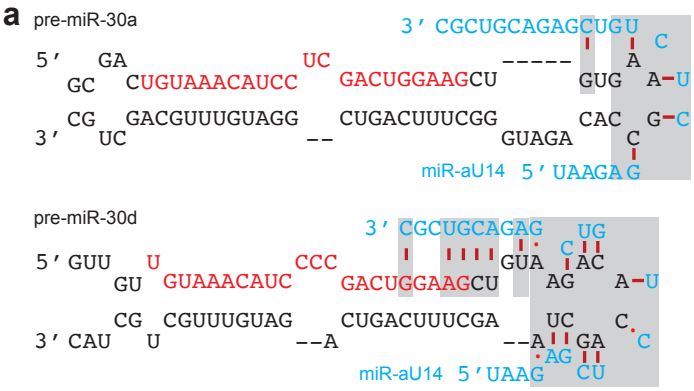

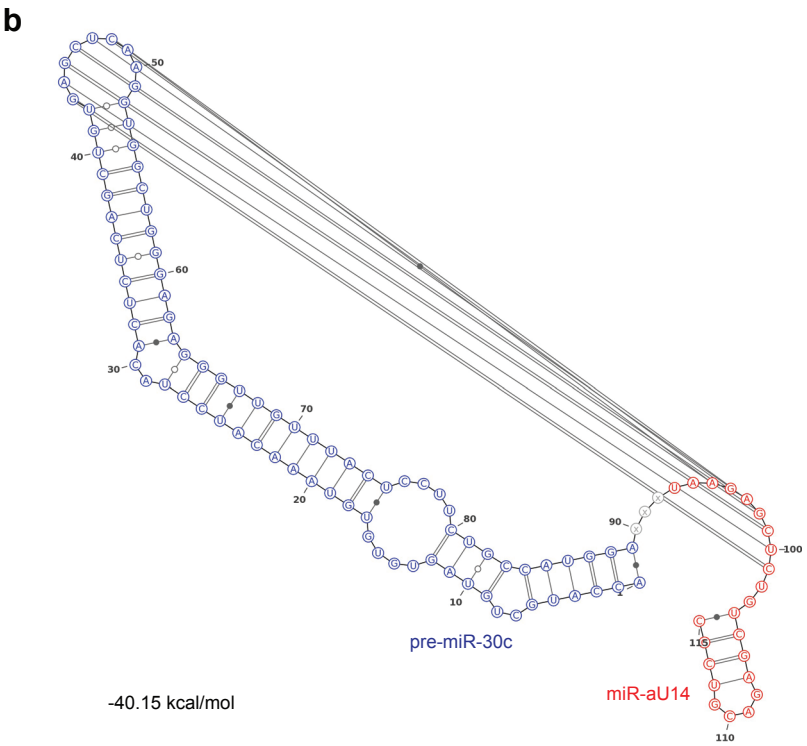

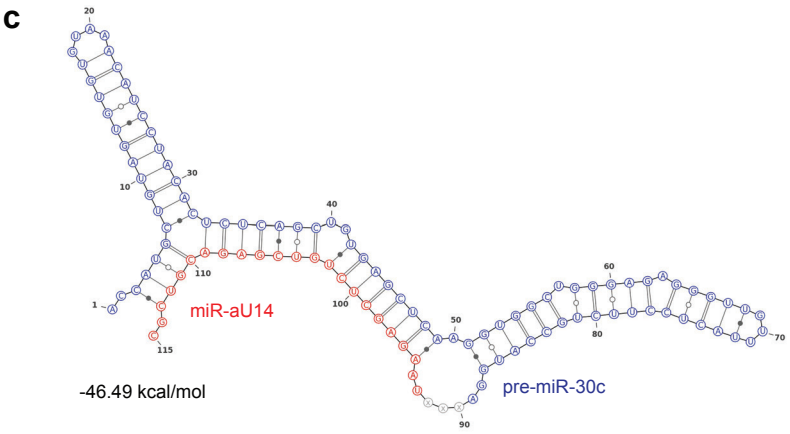

a. Schematic of potential binding site of miR-aU14 in the hairpin loop of different miR-30 family members. Sequence complementarity between miR-aU14 and pre-miR-30a, pre-miR-30d. Potential RNA-RNA interaction regions are highlighted in grey. Mature miR-30 sequences are indicated in red. miR-aU14 is represented in blue. **b, c.** Two different possible conformations (**b** and **c**) for the interaction between miR-aU14 and pre-miR-30c were predicted by VfoldCPX 2D RNA analysis. Free binding energies for respective conformations as predicted by the software are indicated.

Extended data Fig 4: Characterizaion of HHV-6 encoded miR-aU14.

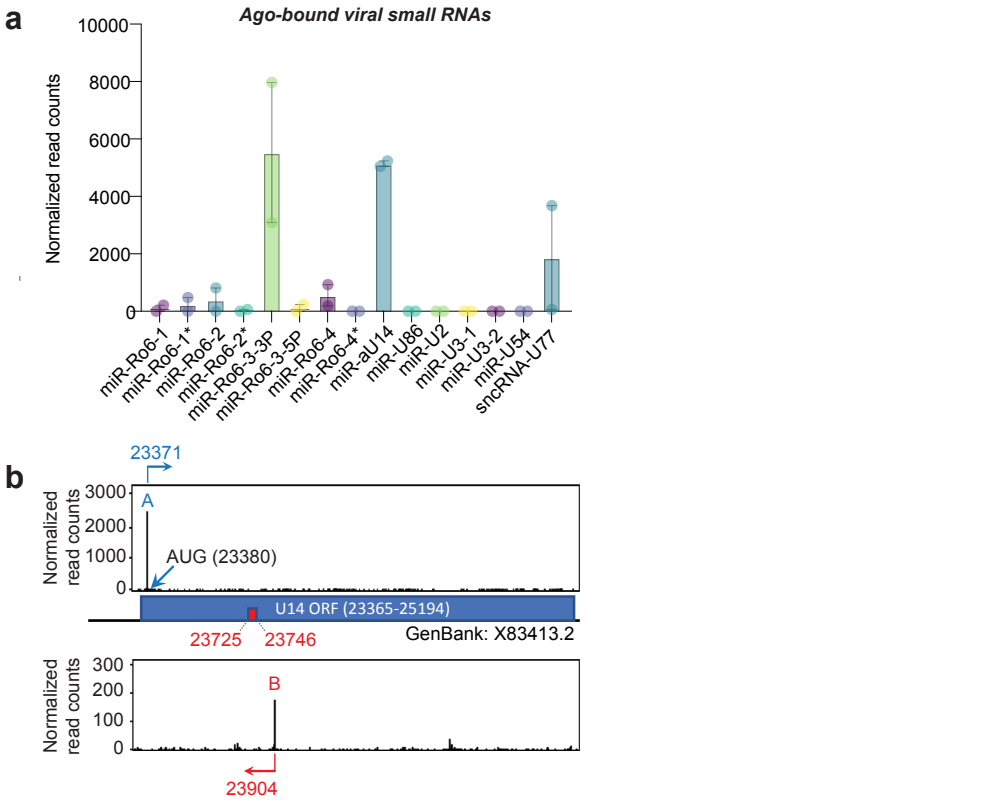

a. Identification of Ago-bound viral miRNAs during lytic HHV-6A infection. HSB-2 cells were infected for 72 h with wild-type HHV-6A. n=3. **b.** dRNA-seq normalized read counts from HSB-2 cells infected with HHV-6A (n=2) are shown for both the sense (upper panel) and antisense (lower panel) strand. Location of miR-aU14 and U14 ORF as well as the identified transcription start sites (TSS) of the U14 mRNA (highlighted as 'A' in blue) and of pri-miR-aU14 (highlighted as 'B' in red) are indicated against the GenBank accession number X83413.2. TSS identified pri-miR-aU14 to initiate 158 nt upstream of miR-aU14 within the first third of the U14 ORF. The TSS that we identified for the U14 mRNA indicates that translation of the U14 ORF only initiates at a second AUG (indicated) that is located 15 nt downstream of the reference AUG. **c.** Predicted folding of pre-miR-aU14. The mature miR-aU14 sequence is highlighted in red. **d.** Putative miR-aU14 sequences from two different strains of HHV-6A (HHV-6A U1102, GenBank X83413.2; HHV-6A GS, GenBank KC465951.1) and one strain of HHV-6B (HHV-6B Z29, GenBank AF157706.1) were aligned. Sequence homology of mature miR-aU14 region is highlighted with red rectangles.

Extended data Fig 5: Viral inhibition of miR-30c processing triggers mitochondrial fragmentation.

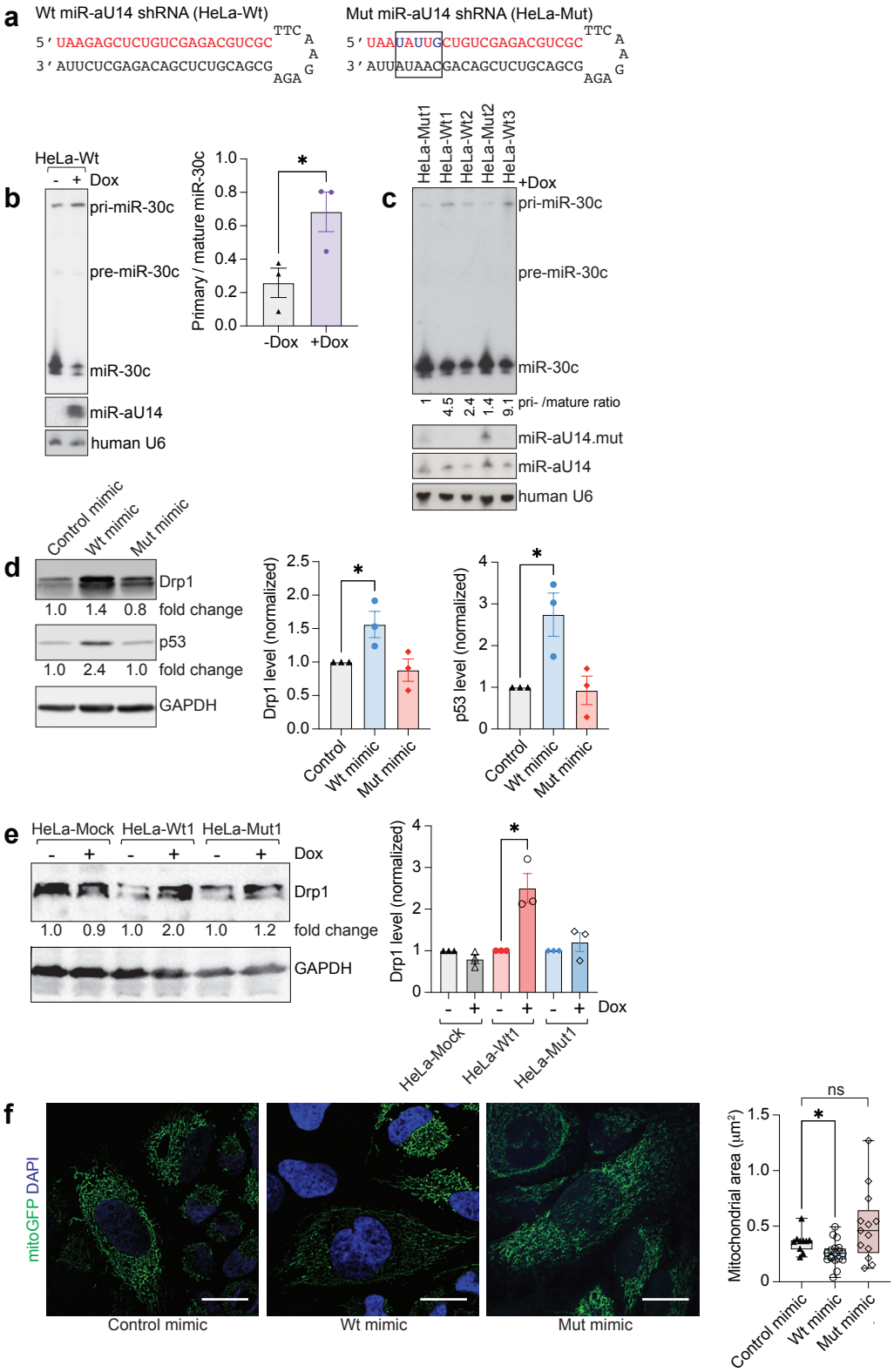

a. Doxycycline-(dox)-inducible wild-type and mutant miR-aU14 shRNAs were expressed in HeLa cells under control of a doxycycline (dox)-inducible Pol III promoter. Mature miR-aU14 sequence is indicated in red. Point mutations are highlighted in blue within a black rectangle. **b.** HeLa cells were stably transduced to express dox-inducible miR-aU14. miR-30c and miR-aU14 expression was probed by Northern blotting. A probe against human U6 served as loading control. Ratio of pri-miR-30c/miR-30c, as determined by densitometric quantification, are shown. n=3. **c.** Polyclonal HeLa cells stably transduced to express either wild-type (HeLa-Wt1, 2 and 3) or mutant (HeLa-Mut1 and 2) miR-aU14 were induced. miR-30c and miR-aU14 expression was probed by Northern blotting. **d.** miR-aU14 mimic induces Drp1 protein expression. Total protein lysates from cells transfected with either a control mimic, miR-aU14 mimic (Wt mimic), or the mutant miR-aU14 mimic (Mut mimic) were subjected to immunoblot analysis for Drp1 and p53 protein levels. **e.** Total protein lysates from polyclonal HeLa cells with dox-inducible wild-type (HeLa-Wt1) or mutant miR-aU14 (HeLa-Mut1) were subjected to immunoblot analysis. **f.** Mitochondrial architecture was studied in U2-OS cells transfected either with miR-aU14 mimic (Wt mimic) or the mutant miR-aU14 mimic (Mut mimic) or a control mimic Fixed cells were counterstained with DAPI. Average mitochondrial area are shown from three independent experiments. n=3. Data are mean ± s.e.m. ns, $P > 0.05$, $*P \leq 0.05$, two-tailed Mann–Whitney U-test (b, d, e), two-way ANOVA with Tukey's multiple comparisons test (f).

Extended data Fig 6: Characterization of miR-aU14 mutant virus.

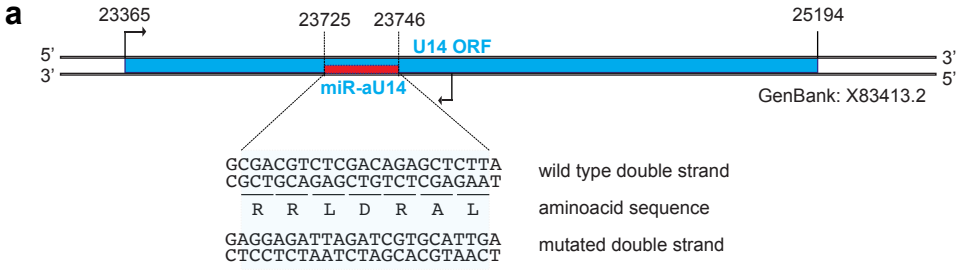

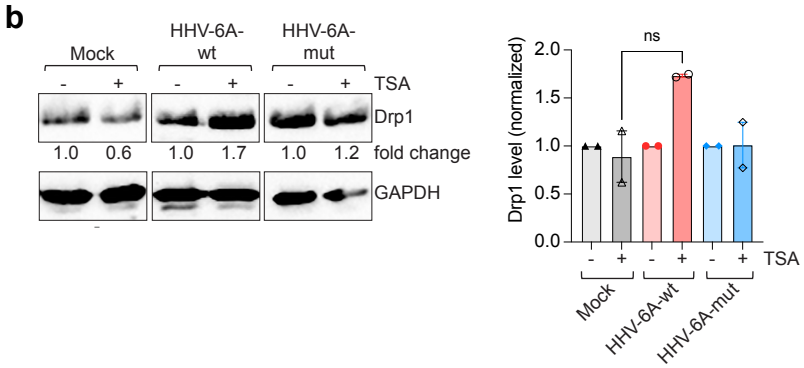

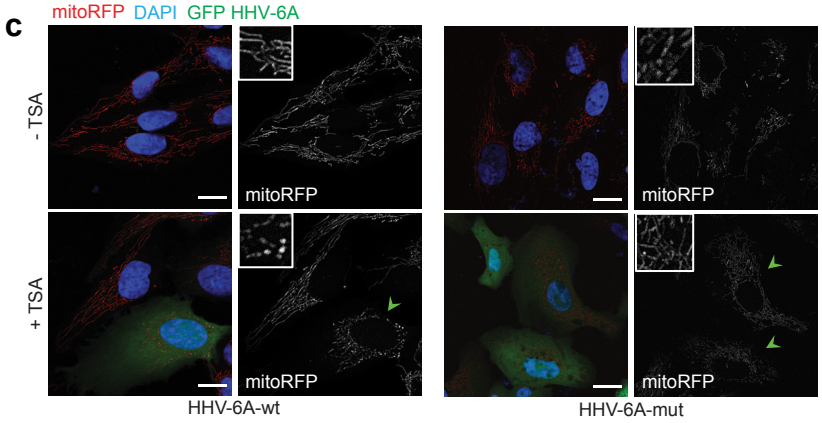

a. The miR-aU14 sequence was altered in the HHV-6A BAC without disturbing the amino acid (aa) sequences of the U14 ORF on the opposing strand. Sequence information at the site of mutation is shown. **b.** HHV-6A reactivation of U2-OS cells carrying latent wild-type (HHV-6A-wt) or miR-aU14 mutant (HHV-6A-mut) HHV-6A genomes was stimulated for 48 h using TSA. U2-OS cells without latent HHV-6A served as mock. Total protein lysates were subjected to immunoblot analysis. GAPDH was used as loading control. Normalized fold change in Drp1 protein levels are presented as a bar diagram. n=2. **c.** Mitochondrial architecture in wild-type or mutant HHV-6A reactivating cells (green arrowheads) carrying stable RFP within mitochondria (mitoRFP). The BAC-derived HHV-6A backbone carries a GFP expression cassette facilitating expression of GFP upon virus reactivation. DAPI as counterstaining. Scale bars represent 10 µm. Data are mean ± s.e.m. ns, $P > 0.05$, two-tailed Mann–Whitney U-test (b).

Extended data Fig 7: miR-aU14 regulates virus lytic/latent switch.

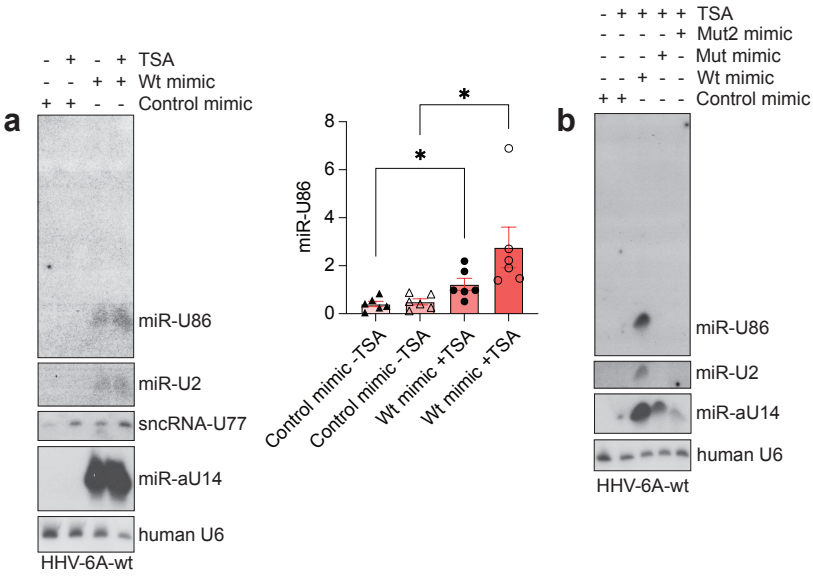

a. U2-OS cells carrying wild type HHV-6A miR-aU14 (HHV-6A-wt) were transfected with either the miR-aU14 mimic or a control mimic. Cells were induced with TSA and the extent of virus reactivation was analyzed by Northern blotting for viral miR-U2, miR-U86 and sncRNA-U77. Human U6 normalized miR-U86 levels from six independent experiments are presented in a bar diagram. n=6. **b.** U2-OS cells carrying latent wild-type HHV-6A were transfected with miR-aU14 mimic or the two mutant miRNA mimics. Cells were induced with TSA and the extent of virus reactivation was analyzed by Northern blotting for viral miR-U86, miR-U2. A probe against human U6 was used as loading control. Data are mean ± s.e.m. *$P \leq 0.05$, two-tailed Mann–Whitney U-test and two-way ANOVA with Tukey's multiple comparisons test (a).

Extended data Fig 8: Human let-7f1 processing can be selectively inhibited by synthetic small RNAs.

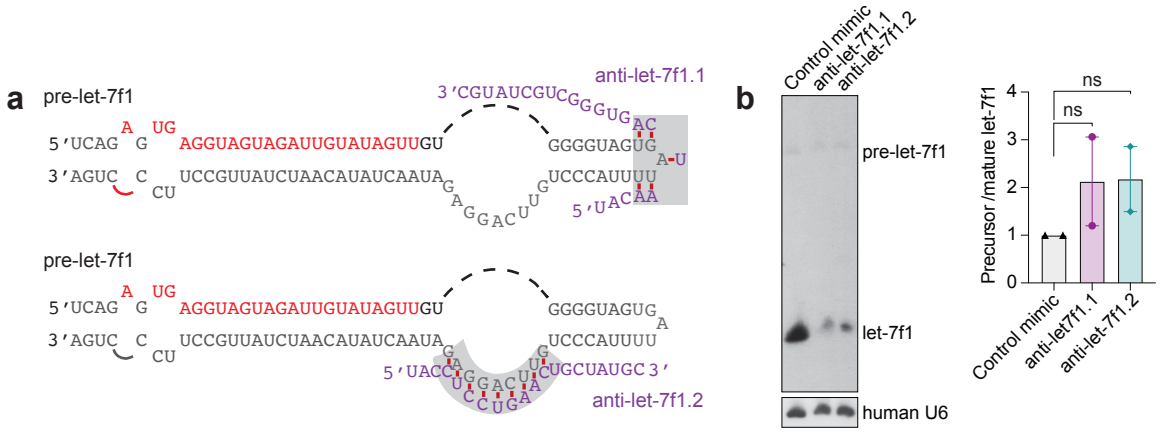

a. Schematic of putative binding of two different synthetic miRNAs to human pre-let-7f1. **b.** Targeting the hairpin loop of pre-let-7f1 with synthetic miRNAs interferes with miRNA processing. Two different miRNA mimics designed against the hairpin loop of pre-let-7f1 or control mimic were transfected into U2-OS cells. let-7d miRNA levels were quantified by Northern blotting. A probe against human U6 was used as loading control. Pre-let-7f1 / let-7f1 ratio, as determined by densitometric analysis, are shown in the bar diagram. n=2. Data are mean ± s.e.m. ns, *P > 0.05*, two-tailed Mann–Whitney U-test (b).

Extended data Fig 9: Graphical abstract of regulation of miRNA-mediated miRNA processing.

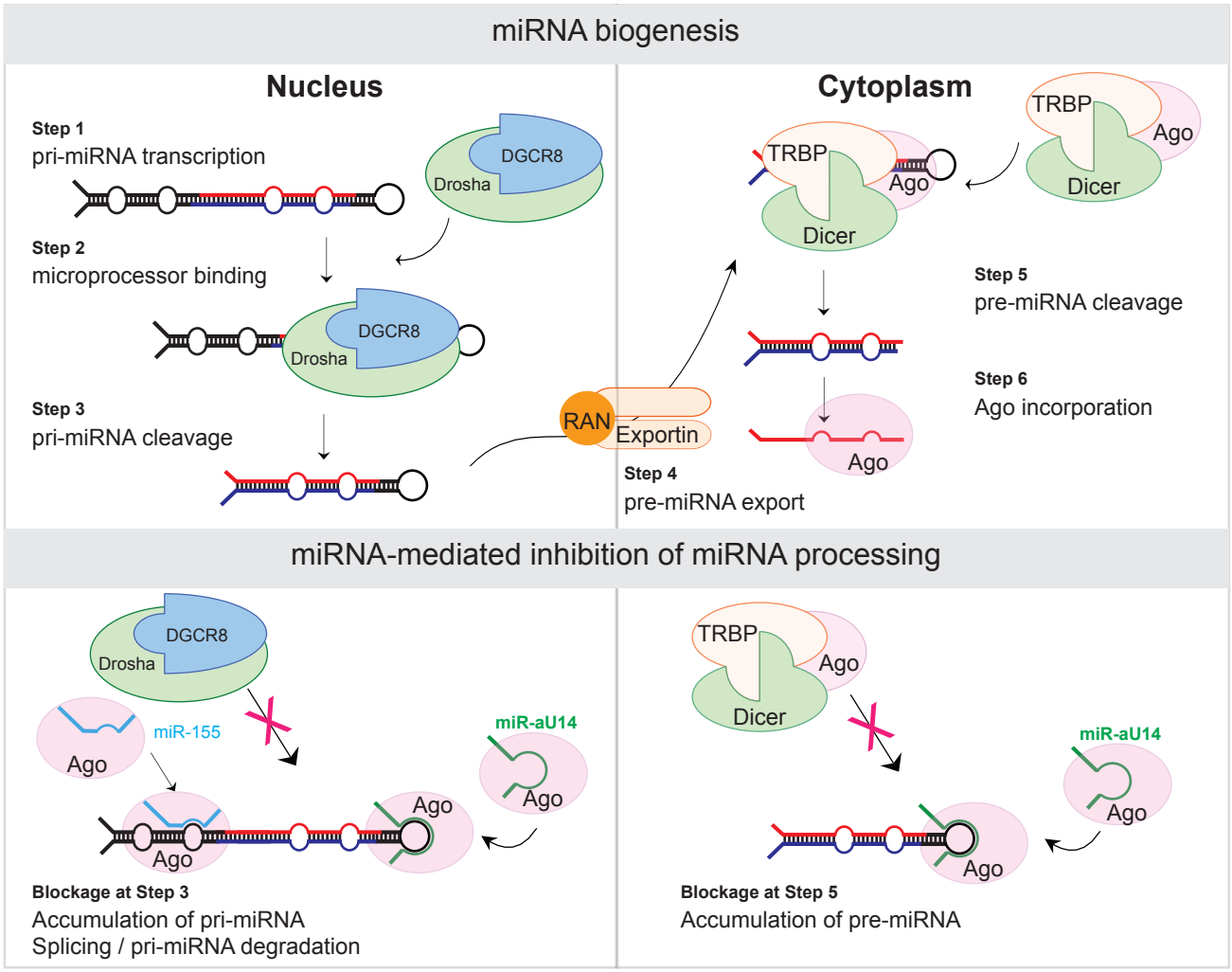

Schematic of regulation of miRNA processing by other miRNAs.